Hot exospheres seen in other giant planetary atmospheres are likely produced by mechanisms similar to those on Jupiter.

REFERENCES AND NOTES

1. M. C. Festou *et al.*, *J. Geophys. Res.* **86**, 5715 (1981).
2. D. F. Strobel and G. R. Smith, *J. Atm. Sci.* **30**, 718 (1973).
3. G. R. Smith *et al.*, *J. Geophys. Res.* **88**, 8667 (1983).
4. F. Herbert *et al.*, *ibid.* **83**, 15093 (1987).
5. A. L. Broadfoot *et al.*, *Science* **246**, 1459 (1989).
6. D. M. Hunten and A. J. Dessler, *Planet. Space Sci.* **25**, 817 (1977).
7. S. K. Atreya *et al.*, *Geophys. Res. Lett.* **6**, 10795 (1979).
8. R. V. Yelle *et al.*, *J. Geophys. Res.* **101**, 2149 (1996).
9. A. Nishida and Y. Watanabe, *ibid.* **86** (no. A12), 9945 (1981); S. K. Atreya, T. M. Donahue, and M. C. Festou, *Astrophys. J.* **247**, L43 (1981).
10. A. Seiff *et al.*, *Science* **272**, 844 (1996). All altitudes in this paper refer to the 1-bar level.
11. G. Orton *et al.*, *ibid.*, p. 839.
12. Personal communication from J. Neff. These parameters are for an altitude of 450 km, the probe entry altitude as defined by the Probe Project Office. They were derived from radio tracking of the orbiter, measurement of the probe separation impulse, the equations of motion, and a model of Jupiter's gravity field. Latitude and longitude at the entry altitude were 6.5303°N and 4.9403°W in System III coordinates, with heading angle 92.6111° clockwise from north. We extended this trajectory upward to the altitude of first data acquisition, where relative velocity and path angle were 47.1303 km/s and 10.6218°, respectively.
13. A. Seiff, E. Venkatapathy, B. Haas, P. Intrieri, *AIAA-96-2451*, 14th AIAA Applied Aerodynamics Conference, New Orleans, LA, 17 to 20 June 1996.
14. Sensors were Bell Model XI guidance accelerometers. To preserve precision over a wide dynamic range, four measurement ranges were implemented with 12-bit digital resolution [A. Seiff and T. C. D. Knight, *Space Sci. Rev.* **60**, 203 (1992)]. Resolution was 3.1×10^{-6} *g* on the most sensitive range; 0.1 *g* on the least sensitive. The first data point retained in memory was 2.057×10^{-4} m/s^2 or 21×10^{-6} *g*. Peak deceleration was 2240 m/s^2 (228 *g*), at an altitude of 101 km above the 1 bar level. (*g* denotes Earth sea-level acceleration of gravity, 9.80665 m/s^2.) An excellent data set was realized, exceeding in both accuracy and altitude and measurement resolution those from a similar experiment at Venus [A. Seiff and D. B. Kirk, *J. Geophys. Res.* **96**, 11,021 (1991); *Icarus* **49**, 45 (1982)].
15. J. N. Moss and A. L. Simmonds, in *Progress in Astronautics and Aeronautics* , P. E. Bauer and H. E. Collicott, Eds. (AIAA, New York, 1983), pp. 419-445.
16. F. S. Milos, *AIAA-96-1823*, 31st AIAA Thermophysics Conference, New Orleans, LA, 17 to 20 June 1996.
17. Below the homopause, composition was based on measurements in the lower atmosphere by the neutral mass spectrometer [H. B. Niemann *et al.*, *Science* **272**, 846 (1996)] and the helium abundance detector (U. von Zahn *et al.*, *ibid.*, p. 849). Above the clouds, where H_2O and NH_3 have been removed by condensation, we selected 0.8625, 0.1358, and 0.0017 for the mole fractions of H_2, He, and CH_4. The homopause, formally, the altitude of equal turbulent and molecular diffusion, is at 370 km. Above the homopause, we calculate the composition assuming diffusive equilibrium [S. K. Atreya, *Atmospheres and Ionospheres of the Outer Planets and Their Satellites* (Springer-Verlag, New York, 1986), p. 89] with a turbulent diffusion coefficient of 5×10^6 cm^2/s [R. J. Vervack *et al.*, *Icarus* **114**, 163 (1995)]. Heavy constituent mole fractions are reduced by diffusive separation to 0.028 (He) and 7×10^{-7} (CH_4) at 500 km, and essentially vanish at 1000 km, while atomic H rises to 0.031 at 1000 km. The gas constant varies from 2.35 J/kg K below the homopause to 1.99 J/kg K at 1000 km.
18. L. A. Young, R. V. Yelle, R. E. Young, A. Seiff, and D. B. Kirk, *Science* **276**, 108 (1997).
19. This resulted from 53 s late deployment of the probe parachute [R. E. Young, M. A. Smith, C. K. Sobeck, *ibid.* **272**, 837 (1996)].
20. R. Hanel *et al.*, *ibid.* **204**, 972 (1979); V. Kunde *et al.*, *Astrophys. J.* **263**, 443 (1982).

22 January 1997; accepted 14 March 1997

Equatorial X-ray Emissions: Implications for Jupiter's High Exospheric Temperatures

J. H. Waite Jr.,* G. R. Gladstone, W. S. Lewis, P. Drossart, T. E. Cravens, A. N. Maurellis, B. H. Mauk, S. Miller

Observations with the High Resolution Imager on the Röntgensatellit reveal x-ray emissions from Jupiter's equatorial latitudes. The observed emissions probably result from the precipitation of energetic (>300 kiloelectron volts per atomic mass unit) sulfur and oxygen ions out of Jupiter's inner radiation belt. Model calculations of the energy deposition by such heavy ion precipitation and of the resulting atmospheric heating rates indicate that this energy source can contribute to the high exospheric temperatures (>800 kelvin at 0.01 microbar) measured by the Galileo probe's Atmospheric Structure Instrument. Low-latitude energetic particle precipitation must therefore be considered, in addition to other proposed mechanisms such as gravity waves and soft electron precipitation, as an important source of heat for Jupiter's thermosphere.

X-rays from Jupiter's northern and southern auroral zones are believed to be line emissions from precipitating sulfur and oxygen ions (*1–4*). Observations made in July 1994 with the High Resolution Imager (HRI) on board the Earth-orbiting Röntgensatellit (ROSAT) reveal, in addition to the expected high-latitude auroral emissions (*5*), well-defined emissions emanating from near Jupiter's equator (*6*), suggesting that energetic ion precipitation occurs at low as well as high latitudes. Charged particle precipitation in the auroral zones, together with Joule heating, is thought to play a major—and perhaps the dominant—role in the global energetics and dynamics of Jupiter's upper atmosphere (*7–9*). Energetic ion precipitation at lower latitudes would thus be expected to have aeronomical effects and must be considered, along with soft electron precipitation at middle and low latitudes (*10*) and breaking gravity waves (*11*), as a possible thermospheric energy source. Such heating mechanisms must be invoked to account for thermospheric temperatures that are much higher than can be explained solely in terms of solar extreme ultraviolet (EUV) heating of Jupiter's upper atmosphere (*12*). Here, we analyze Jupiter's equatorial x-ray emissions, which we assume are excited by precipitating sulfur and oxygen ions, and present calculations of the effects of such energetic ion precipitation on the thermal structure of the jovian equatorial thermosphere.

We observed Jupiter with the ROSAT HRI in July 1994, shortly before and during the impact of comet Shoemaker-Levy 9 (*13*). Although x-ray emissions from Jupiter's equatorial and auroral regions were detected before and during the impact period, we consider for this study only the preimpact data to avoid biasing the analysis by including any unique events associated with the impacts.

Low-latitude x-ray emissions (like those at higher latitudes) are organized in solar local time, occurring predominantly between local noon and dusk in these data (Fig. 1A). Local time organization of the equatorial and auroral x-ray emissions is also evident in HRI observations from March and September 1996. Like the July 1994 observations, the September 1996 observations show that the x-rays emanate principally from the planet's noon-dusk sector. In the case of the March observations, however, the emissions occur preferentially in the morning, rather than the afternoon, sector. The reasons for the local time organization of the jovian x-ray emissions and for the variation between morning and afternoon sectors are not currently understood.

In addition to their organization in local

J. H. Waite Jr., G. R. Gladstone, W. S. Lewis, Department of Space Science, Southwest Research Institute, Post Office Box 28510, San Antonio, TX 78228–0510, USA.
P. Drossart, DESPA, Observatoire de Paris, F-92195 Meudon Cedex, France.
T. E. Cravens and A. N. Maurellis, Department of Physics and Astronomy, University of Kansas, Lawrence, KS 66045–2151, USA.
B. H. Mauk, Applied Physics Laboratory, The Johns Hopkins University, Laurel, MD 20723–6099, USA.
S. Miller, Department of History, Philosophy, and Communication in Science, University College London, London WC1E 6BT, UK.

*To whom correspondence should be addressed. E-mail: hunter@kronos.space.swri.edu

time, the equatorial x-ray emissions also appear to be organized in terms of surface magnetic field strength. They occur largely between 210° and 60° (System III longitude), inside a broad region of low field strength along Jupiter's magnetic dip equator (Fig. 1B). The preferential occurrence of the equatorial emissions within a region of low magnetic field strength is not surprising, because the weak surface magnetic field can be assumed to allow a widened atmospheric loss cone (*14*), resulting in the enhanced interaction of trapped charged particles in the inner radiation belt with Jupiter's upper atmosphere (*15*).

No measurements have been made of the charged particle populations in Jupiter's inner magnetosphere in the relevant energy ranges (*16*). However, we assumed that the low-latitude x-ray emissions are excited by precipitating sulfur and oxygen ions with energies >300 keV amu^{-1}. This assumption is based on earlier observational and theoretical studies (*1–3, 17*) and is supported by our analysis of Voyager Low Energy Charged Particle instrument data near 5 jovian radii (R_J), which showed that inward diffusion of sulfur and oxygen ions near the inner edge of the Io plasma torus can supply the population of charged particles needed to account for the observed emissions (*18*). The amount of energy deposited in Jupiter's low-latitude thermosphere by heavy ion precipitation can be estimated from the x-ray power output, which we calculated to be 10^9 W (*19*). If an efficiency of 0.8×10^{-4} for all charge states is assumed (*3*), this total x-ray output power yields an energy flux of ~0.4 erg cm^{-2} s^{-1} into the observed emission region (−30° to +30° latitude). The inferred power input by low-latitude energetic particle precipitation is $\sim 1.3 \times 10^{13}$ W, a value smaller than but comparable with estimates of auroral power input derived from analyses of observations of Jupiter's ultraviolet aurora (*20*).

To investigate the effect of low-latitude charged particle precipitation on the thermal structure of Jupiter's upper atmosphere, we used a one-dimensional aeronomical model of an outer planet thermosphere-ionosphere (*7, 21*). We considered only heat transport by conduction (*22*) and calculated a neutral temperature profile according to the heat conduction equation

$$\frac{\partial}{\partial z}\left(K\frac{\partial T}{\partial z}\right) = H_z - C_z \qquad (1)$$

where z is altitude, T is the temperature, K is the thermal diffusion coefficient for H_2 (*23*), and H_z and C_z are the local heating and cooling rates (in erg cm^{-3} s^{-1}), respectively.

We assumed that heating processes associated with heavy ion precipitation were the sole source of heat for the jovian thermosphere. Such processes include direct heating by impact-induced dissociation of H_2, electron heating, vibrational excitation, and heating from chemical reactions involving H_2^+ and have a combined heating efficiency of ~50% (*24*). Using the energy flux derived from the observed x-ray output power (~0.4 erg cm^{-2} s^{-1}) and a heating efficiency of 50%, we obtained a vertically integrated neutral heat flux of ~0.2 erg cm^{-2} s^{-1}. For comparison, the solar EUV heat input is 0.06 erg cm^{-2} s^{-1} (on the day side) (*7*), and breaking gravity waves are thought to be able to provide up to 3 erg cm^{-2} s^{-1} (*11*).

The altitude at which energy deposition occurs is crucial to the temperature profile. Heating near the homopause, where cooling by hydrocarbons is efficient, will have little effect. Heating far above the homopause, even a small amount, will have a large effect. Unfortunately, however, the altitude range over which the incoming energetic ions deposit their energy and heating occurs is not known. Therefore, we considered two limiting cases: (i) a low-altitude case, in which particle energy is deposited rapidly in one passage as the particles penetrate directly into the atmo-

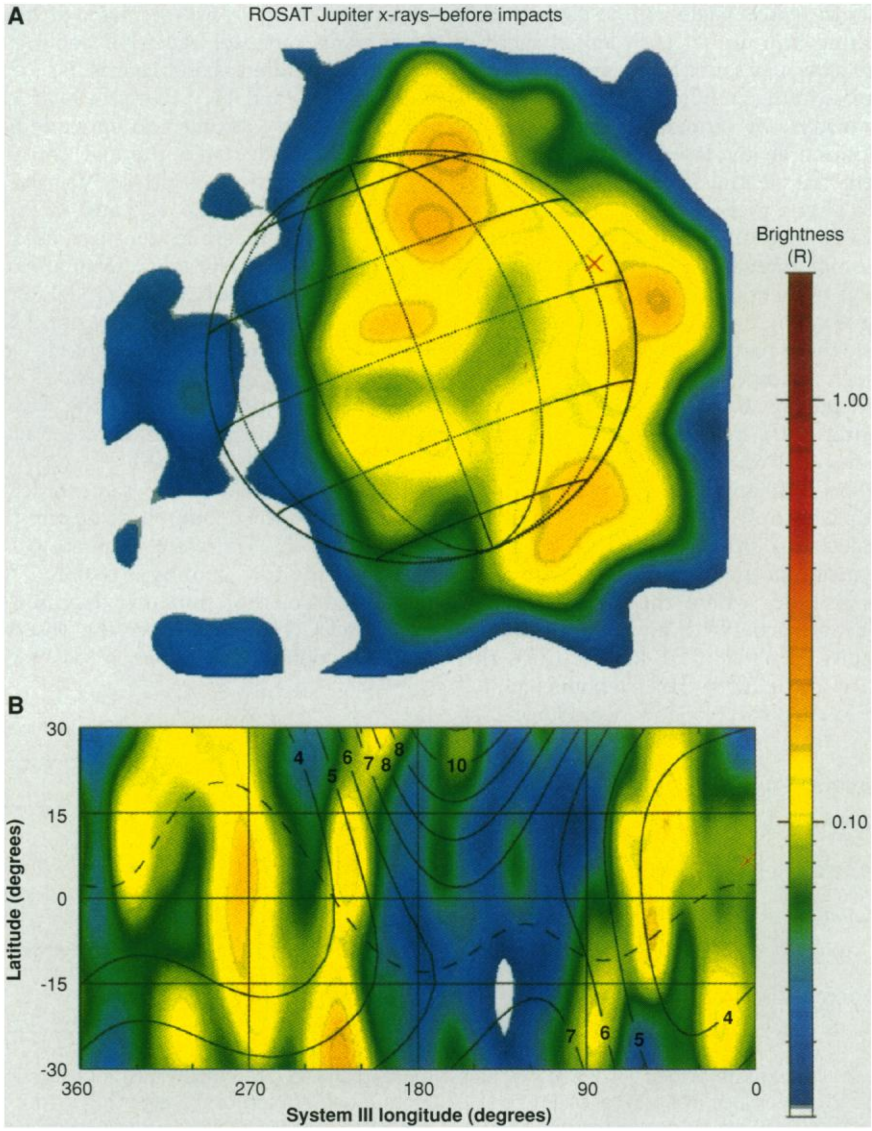

Fig. 1. (**A**) HRI x-ray image of Jupiter, produced with data obtained during 13 through 15 July 1994. Individual photons have been smoothed by the HRI point-spread function (PSF) and converted to brightness units. A graticule showing Jupiter's orientation with 30° intervals in latitude and longitude is overlaid. The red "x" marks the entry site of the Galileo probe in local time. (**B**) HRI x-ray map of Jupiter, produced with the data from (A), but with each PSF-smeared photon mapped into System III longitude and latitude. Contour lines show O6 model (*36*) surface magnetic field strength (in gauss). The dashed line indicates the magnetic dip equator. The red "x" marks the entry site of the Galileo probe. In both (A) and (B), false color indicates emission brightness in Rayleighs (*37*).

sphere and (ii) a high-altitude case in which trapped particles lose energy gradually during multiple bounces between mirror points (*14*).

In a low-altitude case, most of the ions responsible for the observed x-ray emissions will deposit their energy rapidly as they penetrate Jupiter's upper atmosphere. At high latitudes, peak energy deposition by a vertically incident isotropic flux of ≥ 300 keV/amu oxygen ions will occur at an altitude where the atmospheric density is about 3×10^{13} cm^{-3} (*3*). Near the equatorial region, however, the path length will increase by about a factor of 2 because of the dip angle of the magnetic field. Moreover, for weak pitch-angle diffusion into the loss cone, the pitch angle will be close to 90°, resulting in a further path length increase by roughly a factor of 5. Assuming a 10-fold increase in the path length as result of these two factors, we estimate that peak energy deposition at low latitudes will thus occur where the neutral density is $\sim 3 \times 10^{12}$ cm^{-3} or at a pressure of about 85 nbar.

In a high-altitude case, an extended region of gradual energy loss may exist for a large number of trapped ions in the inner magnetosphere. Near the edge of the loss cone, these particles will mirror at a high enough altitude that they deposit only a small portion of their energy at each encounter with the atmosphere. The pressure level at which this energy loss occurs can be estimated by requiring that the particle entirely lose its energy in the time it takes to diffuse radially inward across the magnetic field lines that map to the low latitudes where the x-ray emissions were observed. With an inward diffusion velocity of about 0.01 km s^{-1} (*25*), this time is about 10^6 s. Given a bounce period of ~ 5 s, about 10^5 bounces could occur, so that the atmospheric density for the ion energy deposition should be about this factor less than if the ions deposited their energy directly in one passage. This gives a neutral density of about 3×10^7 cm^{-3} or a pressure of about 5×10^{-3} nbar.

We adopted a two-parameter heating rate formula to represent the high-altitude and low-altitude cases in Eq. 1. We specified the column heating rate for each profile and made the heating rate proportional to the atmospheric pressure down to a critical pressure level below which the heating rate was set equal to zero. The critical level was 2×10^{-9} bar for the high-altitude case and 8.5×10^{-8} bar for the low-altitude one. To obtain the cooling term used in Eq. 1, we calculated altitude-dependent rates for radiative cooling by thermal infrared band emissions from CH_4, C_2H_2, and H_3^+. For the hydrocarbon species, we assumed an optically thin regime and calculated thermal emission rates as a function of altitude for the ν_4 band of CH_4 and the ν_5 band of C_2H_2 (*26*). The hydrocarbon densities used in our calculations were taken from a recent hydrocarbon photochemistry model for Jupiter's North Equatorial Belt region (*27*).

Thermal infrared emissions of H_3^+ observed at equatorial latitudes (*28*, *29*) are much weaker than those in the auroral zone, but they nonetheless represent a column cooling rate of ~ 0.1 erg cm^{-2} s^{-1} (*29*), which is about the same order of magnitude as the column heating rate (0.2 erg cm^{-2} s^{-1}). Therefore, accurate calculation of the H_3^+ cooling is required. We employed a method similar to that used for CH_4 and C_2H_2. To achieve the observed column cooling rate values, it was necessary to invoke a reaction rate coefficient of 3.4×10^{-10} cm^3 s^{-1} for the translation-vibration reaction $H_2^* + H_3^+ \rightarrow H_2 + H_3^+(v)$. This rate is consistent with the Langevin (gas kinetic) rates typical of atom transfer reactions. To calculate H_3^+ density, we used our one-dimensional model of the jovian ionosphere (*7*, *21*), updated to include a new neutral atmosphere derived from the Galileo probe Atmospheric Structure Instrument (ASI) data, revised ion production rates for energetic ion precipitation, and a revised rate for the reaction of H^+ with vibrationally excited H_2 ($v \geq 4$), an important loss process for this ion in the jovian ionosphere (*30*). The rates for particle-induced ionization and high-altitude heating were consistent with each other within the uncertainties of the model (Table 1) and yielded an ionospheric profile that is consistent with the equatorial ionospheric profile derived from Voyager radio occultation data (*31*). The calculated column density for H_3^+ is 10^{11} cm^{-2}.

Our calculated heating and cooling rate profiles are shown in Fig. 2. H1 is the heating rate profile for the low-altitude case, with a base of 85 nbar; H2 is the profile for the high-altitude case, with a base of 2 nbar. We used a column-integrated heating rate of 0.2 erg cm^{-2} s^{-1} to calculate both profiles. This is the rate that is most consistent with the ion energy flux calculated on the basis of the observed x-ray output power. A third heating rate profile (H3), also for the high-altitude case but with two times our preferred column heating rate (that is, 0.4 erg cm^{-2} s^{-1}), is shown as well. The column cooling rate profiles for the hydrocarbons and for H_3^+ (~ 0.1 erg

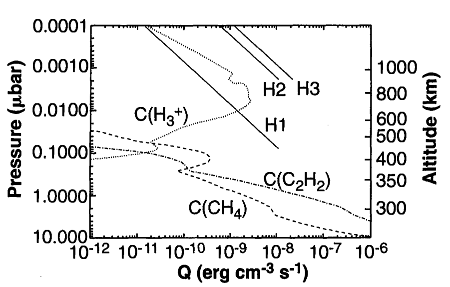

Fig. 2. Heating rate profiles for the low-altitude (H1) and high-altitude (H2, H3) cases. H1 and H2 were calculated with the column-integrated heating rate (0.2 erg cm^{-2} s^{-1}) most consistent with the observed x-ray emissions; H3 is the profile obtained when a heating rate two times the preferred value was used (that is, 0.4 erg cm^{-2} s^{-1}). The associated calculated cooling rate profiles (indicated by C) for hydrocarbons below the homopause (CH_4 and C_2H_2) and for H_3^+ in the ionosphere are also shown.

Table 1. Heavy ion energy deposition in Jupiter's equatorial upper atmosphere.

Parameter	Preferred value	Range
Emitted x-ray power	1×10^9 W	$0.5–2.0 \times 10^9$ W
X-ray production efficiency	0.8×10^{-4}	$0.1–1.0 \times 10^{-4}$
Estimated input power	1.3×10^{13} W	$5 \times 10^{12}–2 \times 10^{14}$ W
Heating efficiency	0.5	0.45–0.6
Column-integrated heating rate	0.2 erg cm^{-2} s^{-1}	0.08–3 erg cm^{-2} s^{-1}

Fig. 3. Model temperature profiles corresponding to the heating and cooling rates of Fig. 2. The dashed and solid lines show the profiles resulting from a heating rate of 0.2 erg cm^{-2} s^{-1} for the low-altitude and high-altitude cases, respectively. The dotted line shows the high-altitude profile obtained for a heating rate of 0.4 erg cm^{-2} s^{-1}. The asterisk line shows the temperature profile extracted from the density profile measured by the Galileo probe (*33*). (It should be noted that the temperatures retrieved from the probe data become substantially uncertain at pressures <0.01 μbar.)

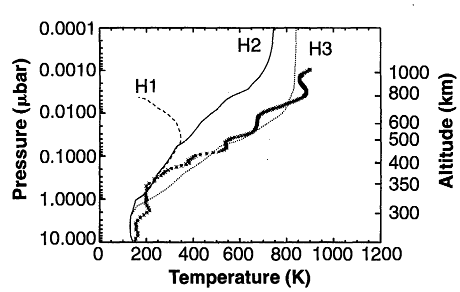

cm^{-2} s^{-1}) are consistent with Voyager infrared interferometer spectrometer (IRIS) and Infrared Space Observatory/Short Wavelength Spectrometer (ISO/SWS) observations (*8*, *32*) and with observations of equatorial H_3^+ emissions (*29*), respectively.

To assess the effectiveness of heavy ion precipitation as a heat source for Jupiter's equatorial upper atmosphere, we compared our model temperature profiles with the thermospheric temperature profile derived from the Galileo probe ASI density data (*33*). The ASI measurements were made at a location (+6.54° and 4.46° System III longitude) and a local time (22:04:16 UTC = ~1600 solar local time) (*34*) at which, according to the ROSAT observations, strong heating of the atmosphere by heavy ion precipitation would be expected (*35*). Comparison of the ASI-derived thermal profile with the model profiles calculated for an assumed heating rate of 0.2 erg cm^{-2} s^{-1} (Fig. 3, curves H1 and H2) demonstrates that heavy ion precipitation can contribute to the heating of Jupiter's equatorial thermosphere. As expected (because the energy deposition occurs well above the hydrocarbon cooling layer), the high-altitude source (H2) produces a larger temperature enhancement than does the low-altitude source (H1). To achieve the best fit to the heating indicated by the probe data, high-altitude heating with a heating rate roughly two times that of our preferred value is required (H3). Although this larger value falls within the uncertainties of our calculations (Table 1), it represents a heating rate that is somewhat greater than would be expected in light of our energy input calculations. Thus, whereas heavy ion precipitation could possibly account for all of the heating observed by the Galileo probe, other heating mechanisms—such as upward-propagating gravity waves (*11*) and supersonic jets driven by auroral energy deposition (*9*)—must also be considered. In any case, with an input power of approximately 1.3×10^{13} W, which is only a few times smaller than the dominant auroral zone thermospheric heat source, low-latitude energetic ion precipitation must be regarded as a significant influence on the structure and circulation of Jupiter's upper atmosphere, both locally and globally.

REFERENCES AND NOTES

1. A. E. Metzger *et al.*, *J. Geophys. Res.* **88**, 7731 (1983).
2. J. H. Waite *et al.*, *ibid.* **99**, 14788 (1994).
3. T. E. Cravens *et al.*, *ibid.* **100**, 17153 (1995). The x-ray production efficiency can range from 0.1 to 1.0 $\times 10^4$.
4. Electron bremsstrahlung has also been proposed to account for the jovian x-rays [D. D. Barbosa, *ibid.* **95**, 14969 (1990)]; however, the arguments advanced in support of this mechanism have been challenged as being inconsistent with the theory of secondary electron production in the terrestrial aurora [J. H. Waite, *ibid.* **96**, 19529 (1991)].
5. J. H. Waite *et al.*, *Science* **268**, 1598 (1995). These observations were made just before and during the impact of comet Shoemaker-Levy 9 with Jupiter. Brightenings of the high-latitude x-ray emissions were observed in association with the impacts of comet fragments K and P2.
6. J. H. Waite *et al.*, in *Röntgenstrahlung from the Universe*, Proceedings of the International Conference on X-ray Astronomy and Astrophysics (MPE Report 263), Würzburg, Germany, 25 to 29 September 1995, H. U. Zimmermann *et al.*, Eds. (Max-Planck-Institut für Extraterrestrische Physik, Garching, Germany, 1996), p. 641.
7. J. H. Waite *et al.*, *J. Geophys. Res.* **88**, 6143 (1983).
8. P. Drossart *et al.*, *ibid.* **98**, 18803 (1993).
9. J. Sommeria *et al.*, *Icarus* **119**, 2 (1995).
10. D. M. Hunten and A. J. Dessler, *Planet. Space Sci.* **23**, 817 (1977).
11. R. G. French and P. J. Gierasch, *J. Atmos. Sci.* **31**, 1707 (1974); R. V. Yelle *et al.*, *J. Geophys. Res.* **101**, 2149 (1996).
12. R. J. W. Henry and M. B. McElroy, *J. Atmos. Sci.* **26**, 912 (1969); D. F. Strobel and G. R. Smith, *ibid.* **30**, 718 (1973). Solar EUV heating can account for a rise of only a few degrees in the temperature of the upper atmosphere above the stratosphere. Jupiter's high thermospheric temperature was first discovered through the analysis of Pioneer 10 radio occultation data [S. K. Atreya and T. M. Donahue, in *Jupiter: Studies of the Interior, Atmosphere, Magnetosphere, and Satellites*, T. Gehrels, Ed. (Univ. of Arizona Press, Tucson, AZ, 1976), pp. 304–318].
13. A total of 63.058 ks of data were acquired—25.655 ks before the impact period and 37.403 ks during the impact period. The photons were time-tagged, making it possible to compensate for the relative motion of Jupiter and the spacecraft and to produce—within the uncertainties imposed by the pointing accuracy and imager point spread function—images of the emission regions within the disk of Jupiter. Knowledge of the positions of the optical counterparts of two x-ray point sources identified within the ROSAT field-of-view (diameter = 40 arc min) reduced the pointing uncertainty from 5 arc sec to ≤3 arc sec. The spatial resolution was still limited by the HRI point spread function (6.5-arc-sec diameter for a 95% power circle), but it was better than that of past HRI observations owing to the more accurate pointing. For information on the HRI point spread function, see L. P. David *et al.* [in *The ROSAT High Resolution Imager* (U.S. ROSAT Science Data Center and Smithsonian Astrophysical Observatory, Cambridge, MA, 1995), pp. 6–13]. The details of the method used to improve the pointing uncertainty are given in note 10 in (*5*). To eliminate possible contamination by ultraviolet emissions, only data from channels ≥4 of the HRI were used in creating the images.
14. Trapped charged particles bounce back and forth along magnetic field lines between "mirror points" in the northern and southern hemispheres. The altitude at which the mirror points occur and the particles reverse direction depends on the strength of the magnetic field (which increases as the field lines converge) and on the equatorial "pitch angle" of the particle—that is, upon the angle between the velocity vector of the charged particle and the magnetic field line along which it is traveling with a gyrating motion. Particles with sufficiently small equatorial pitch angles have mirror points so low that they collide with atmospheric neutrals and are lost. These particles are said to be within the "loss cone." The smaller the surface magnetic field strength, the larger the corresponding loss cone will be.
15. Charged particles in the Earth's Van Allen belts are similarly influenced by a broad minimum in the terrestrial surface field known as the South Atlantic Anomaly [compare W. N. Speldvik and P. L. Rothwell, in *Handbook of Geophysics and the Space Environment*, A. S. Jursa, Ed. (Air Force Geophysics Laboratory, Hanscom AFB, MA, 1985), p. 5.1].
16. The Galileo probe measured high-energy (on the order of several to hundreds of MeV/amu) charged particles at 5, 4, and 3 R_J and continuously between 2.4 and 1.25 R_J [H. M. Fischer *et al.*, *Science* **272**, 856 (1996)]. However, the energies of the particles responsible for the x-ray emissions are far below those measured by the probe.
17. N. Gehrels and E. C. Stone, *J. Geophys. Res.* **88**, 5537 (1983).
18. This is a different population from the energetic (MeV) heavy ions that have been observed in the outer regions of the Io torus (*17*) and that are lost along field lines connecting the torus to Jupiter's high latitudes. The population responsible for the equatorial x-ray emissions most likely consists of keV heavy ions from the inner torus that are energized by a factor of ~200 through conservation of the first and second adiabatic invariants as they diffuse radially inward from ~5 R_J and that are increasingly restricted to smaller pitch angle variations near 90° (that is, trapped). In calculating the energy deposited by these particles, we assume that there is no pitch angle scattering, whereas we assume strong scattering in the case of the outer torus population. Under these assumptions, the energy deposited in Jupiter's upper atmosphere by both populations is roughly equivalent.
19. About 220 photons were detected from the equatorial regions (latitudes <30°) during the 25,655 s of before impact data. If a photon energy of 300 eV is assumed, an HRI effective area of 30 cm^2 yields a flux at Earth of $\sim 1.4 \times 10^{-13}$ erg cm^{-2} s^{-1}. The total estimated x-ray power emitted by Jupiter (P) is $4\pi d^2$ times this value, where d is the Earth-Jupiter distance (equal to 5.1 AU). Thus P is $\sim 1 \times 10^{16}$ erg s^{-1} or $\sim 1 \times 10^9$ W (0.5 to 2.0×10^9 W).
20. A. L. Broadfoot *et al.*, *J. Geophys. Res.* **86**, 8259 (1981); T. A. Livengood *et al.*, *Icarus* **97**, 26 (1992). Esimated power input ranges from 5×10^{12} to 2×10^{14} W.
21. J. H. Waite, thesis, University of Michigan (1981); J. H. Waite *et al.*, *J. Geophys. Res.* **93**, 7244 (1988).
22. Our knowledge of jovian thermospheric dynamics is still too limited to allow heat transport by dynamical processes, such as turbulence and winds, to be included in our calculations. Because our measurements are approximately global, the redistribution of heat by dynamics should average out, and the heat conduction equation should be valid as a large-scale average.
23. K is equivalent to AT^s, where A = 252 erg cm^{-1} s^{-1} K^{-1} and s = 0.751 [H. J. M. Hanley *et al.*, *J. Res. Natl. Bur. Stand. Sec. A* **74**, 331 (1970)]. A and s are empirical constants for fit to laboratory data.
24. M. Horanyi *et al.*, *J. Geophys. Res.* **93**, 7251 (1988). Heating efficiency can range from 45 to 60%.
25. Diffusive radial transport of charged particles within magnetospheres is generally characterized with a radial diffusion coefficient (D), which acts on the radial gradient of the phase space density of the charged particles [M. Schulz and L. J. Lanzerotti, *Particle Diffusion in the Radiation Belts* (Springer-Verlag, New York, 1974)]. When the phase space density profiles are not known, as in the case of the inner jovian magnetosphere, radial transport can be represented with a "diffusion velocity," defined as $V_D = R \times D/(\Delta L)$ km s^{-1}, where ΔL is the e-folding distance for radial variations in the phase space density (expressed in units of planetary radii), and R is the planetary radius in kilometers. By assuming a diffusion velocity of ~0.01 km s^{-1} (± a factor of 3), we achieve reasonable closure between the ion populations at ~5 R_J [B. H. Mauk, S. A. Gary, M. Kane, E. P. Keath, S. M. Krimigis, *J. Geophys. Res.* **101**, 7685 (1996)] and the x-ray emissions reported here.
26. Infrared emissions from these bands play a dominant role in radiative cooling just above the homopause. The method used to calculate the hydrocarbon cooling rates is described in (*8*). Nonlocal thermodynamic equilibrium effects were accounted for through the use of the cooling-to-space approximation [J. F. Appleby, *Icarus* **85**, 355 (1990)].
27. G. R. Gladstone, M. Allen, Y. L. Yung, *ibid.* **119**, 1 (1996).
28. G. E. Ballester *et al.*, *ibid.* **107**, 189 (1994).
29. H. A. Lam, thesis, University College London (1995).

30. T. E. Cravens, *J. Geophys. Res.* **92**, 11083 (1987).
31. V. R. Eshleman et al., *Science* **204**, 976 (1979); ______, *ibid.* **206**, 959 (1979); J. H. Waite et al., paper presented at 31st COSPAR Scientific Assembly, Birmingham, UK, 14 to 21 July 1996.
32. Th. Encrenaz et al., *Astron. Astrophys.* **315**, L397 (1996).
33. A. Seiff et al., *Science* **272**, 844 (1996); A. Seiff et al., *ibid.* **276**, 102 (1997).
34. R. E. Young, M. A. Smith, C. K. Sobeck, *ibid.* **272**, 837 (1996).
35. Because low-latitude ion precipitation appears to be modulated by System III longitude, measurements made at other longitudes or local times would likely have revealed slightly cooler thermospheric temperatures.
36. J. E. P. Connerney, *J. Geophys. Res.* **98**, 18659 (1993).
37. The Rayleigh (R) is a unit of surface brightness equivalent to an intensity of 10^6 photons cm^{-2} s^{-1} per 4π steradians. The flux received at a detector from a source with brightness B (in Rayleighs) is $F = 10^6 B\omega/4\pi$ (in photons per square centimeter per second), where ω is the solid angle of the source (as seen from the detector) in steradians.
38. We gratefully acknowledge the work of the ROSAT team. ROSAT is supported by the Bundesministerium für Forschung und Technologie. We thank A. Seiff for furnishing the latest temperature profile derived from the ASI data. J.H.W. thanks the Centre National de la Recherche Scientifique and the staffs of the Observatoire de Paris-Meudon and the Observatoire de Midi-Pyrénées, where most of the modeling reported in this paper was performed. J.H.W., G.R.G., and W.S.L. acknowledge support from the ROSAT Guest Observer Program (NAG5-2617) and the NASA Planetary Atmospheres Program (NAGW 3624).

15 October 1996; accepted 30 January 1997

Gravity Waves in Jupiter's Thermosphere

Leslie A. Young,* Roger V. Yelle, Richard Young, Alvin Seiff, Donn B. Kirk

The Atmosphere Structure Instrument on the Galileo probe detected wavelike temperature fluctuations superimposed on a 700-kelvin temperature increase in Jupiter's thermosphere. These fluctuations are consistent with gravity waves that are viscously damped in the thermosphere. Moreover, heating by these waves can explain the temperature increase measured by the probe. This heating mechanism should be applicable to the thermospheres of the other giant planets and may help solve the long-standing question of the source of their high thermospheric temperatures.

The atmospheres of the giant planets (Jupiter, Saturn, Uranus, and Neptune) and Earth reach high temperatures in the low-pressure region of the upper atmosphere known as the thermosphere (*1*). On Earth, the energy to heat the thermosphere is supplied by absorption of solar extreme ultraviolet (EUV) radiation. However, for the giant planets, the solar heating rate is more than one order of magnitude too small to explain the high temperatures. Suggestions for Jupiter's thermospheric heat source include charged particle impacts, Joule heating, or the dissipation of gravity waves (*2, 3, 4*). It has been difficult to evaluate these energy sources because, until recently, the shape of the thermal profile above the 1-μbar level was poorly constrained. Without knowing the first and second derivatives of the temperature profile, it is difficult to estimate the amount of energy required or the altitude at which the energy must be deposited by mechanisms which seek to explain the thermal profile. The Atmosphere Structure Instrument (ASI) directly measured the temperature of Jupiter's upper atmosphere on 7 December 1995 (*5*). The ASI experiment detected wave-like fluctuations superimposed on a 700 K temperature increase in the thermosphere. Here we describe how these temperature fluctuations are consistent with gravity waves, and show that viscous dissipation of these waves can be responsible for the elevated thermospheric temperatures.

We decomposed the ASI temperature profile into a mean profile (Fig. 1A) and perturbations (*6*). Subtracting the mean thermal profile from the observed thermal profile leaves temperature fluctuations, peak-to-peak, of 50 to 80 K. These thermospheric waves have extrema at 940, 800, 665, 550, 495, 447, 425, and 395 km. Taking the distance between extrema as the half period, we estimated an observed vertical wavelength of ~260 km above 550 km, ~100 km between 450 and 550 km, and ~50 km between 395 and 450 km. The mesopause, which is the boundary between the middle atmosphere and the thermosphere, is located at the temperature minimum near 290 km (3.3 μbar). The temperature gradient rises quickly above the mesopause, and reaches a maximum of 2.9 K/km at an altitude of 357 km. The positive thermal gradient implies that an energy of 0.53 $erg/cm^2/s$ is transported downward by thermal conduction. This conductive flux must be balanced by heating in steady state; therefore, the column-integrated heating rate in the thermosphere is also 0.53 $erg/cm^2/s$. The inferred upward flux at the top of the ASI observations is between 0 and 0.1 $erg/cm^2/s$, and depends on the method of defining the mean state (*7*).

We modeled how gravity waves could produce the estimated temperature perturbations under the following assumptions: (i) the frequency of the gravity wave is much larger than the Coriolis parameter, (ii) the mean state varies slowly compared to a wavelength, (iii) the period of the gravity

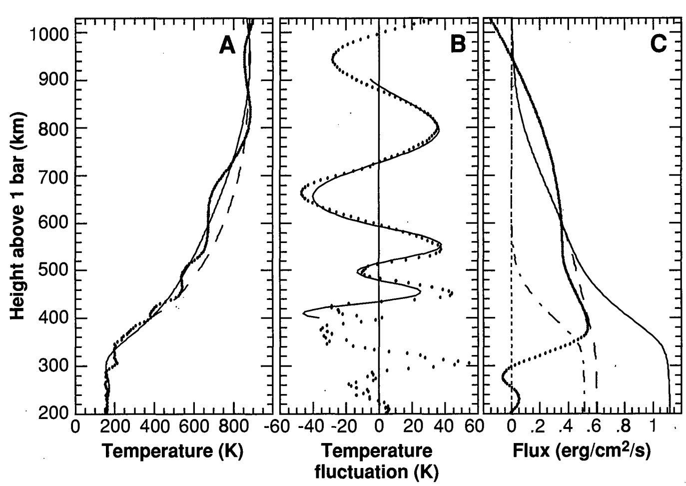

Fig. 1. (**A**) The observed ASI temperatures (thick dotted curve), an estimate of the mean thermal profile (solid curve), and the thermal profile which we ultimately derive by integrating the heating by the observed gravity waves (dashed curve). The dots represent individual measurements by the ASI. (**B**) The temperature fluctuations that remain after subtracting the mean state. The solid curve is the calculated sum of the two gravity waves summarized in Table 1. The dotted curve is the difference between the observed ASI temperatures and the estimated mean thermal profile. (**C**) The dots represent the rate at which energy is conducted downward, derived from the mean thermal profile. The solid curve is the total flux carried upward by the two waves, assuming $\varepsilon F(z_0) = 0.2$ $erg/cm^2/s$ for both waves.

L. A. Young and R. V. Yelle, Center for Space Physics, Boston University, Boston, MA 02215, USA.
R. Young, Space Science Division, NASA Ames Research Center, Moffett Field, CA 94035, USA.
A. Seiff, Department of Meteorology, San Jose State University Foundation, CA 95192, USA.
D. B. Kirk, University of Oregon, Eugene, OR 97403, USA.

*To whom corresponence should be addressed. E-mail: layoung@bu.edu